

Intercalation of oxalate ions in the interlayer space of a layered double hydroxide for nickel ions adsorption

Giscard Doungmo, Théophile Kamgaing *, Ranil Clément Tonleu Temgoua, Ervice Ymele, Francis Merlin Melatagua Tchieno, Ignas Kenfack Tonlé

Laboratory of Noxious Chemistry and Environmental Engineering, Department of Chemistry, Faculty of Science, University of Dschang, P.O. Box 67, Dschang, Cameroon
*Corresponding author E-mail: theophile.kamgaing@univ-dschang.org

Abstract

In this study, sorption properties of a synthesized anionic clay were enhanced by the intercalation of oxalate ions in its interlayer space. The pristine and modified clay materials were characterized by X-ray diffraction, Fourier transform infrared spectroscopy and thermal analysis. These techniques confirmed the presence of oxalate ions in the interlayer space of the clay. The intercalated clay was then used as a matrix for the sorption in batch mode of nickel ions in aqueous solution. The influence of a number of parameters such as contact time, pH, initial concentration of the analyte and adsorbent dosage were studied. The maximum adsorption of nickel was obtained at pH 6, that is, about 90% Ni²⁺ removal. The adsorbent/adsorbate equilibrium follows a pseudo-second order kinetics and best matches the Langmuir model. The modified clay was shown to be efficient matrix for the sorption of nickel ions.

Keywords: Layered Double Hydroxides; Adsorption; Heavy Metals; Oxalate Ions.

1. Introduction

Nickel is a toxic heavy metal widely used in silver refineries, electroplating, zinc base casting and storage battery industries [1-2]. It is an inorganic pollutant of serious concern because of its carcinogenic effects [3]. Since heavy metals are recognized to be non-biodegradable, it is advisable to remove them from industrial wastewater before discharge into the environment.

Several methods such as ion exchange, solvent extraction, reverse osmosis, precipitation, electrochemical and adsorption processes have been proposed for the treatment of sewage contaminated with heavy metals [4-5]. However, the above mentioned methods are not economically feasible for small and medium size industries. It is therefore necessary to search for low cost techniques that may be effective, less environmentally degrading and economical [6].

For water containing small amounts of metal ions, adsorption is recommended for their removal because it is simple, sludge free and involve small initial cost and land investment. Activated carbon is a potential adsorbent for heavy metals in water but the cost of its activation limits its application in developing countries. Therefore, investigating new adsorbents with adsorption capacities and efficiencies comparable to that of commercial activated carbon has been the aim of many research works.

Layered double hydroxides (LDHs), also known as hydrotalcite-like compounds, consist of brucite-like layers which contain the hydroxides of divalent (M^{II}) and trivalent (M^{III}) metal ions and have an overall positive charge balanced by hydrated anions between layers. These compounds present the general formula $[M^{II}_{(1-x)}M^{III}_x(OH)_2]^{x+}(A^{n-})_{x/n} \cdot mH_2O$ where Aⁿ⁻ is the intercalated anion. Because of the strong hydration of these inorganic ions, the interlayer space of LDHs is hydrophilic in nature. As a result, natural clay minerals as well as LDHs show rather weak affinity

towards most ionic metal compounds and are seldom used as sorbents for heavy metals [7-8].

Under suitable conditions, the inorganic ions in clay minerals and LDHs can be replaced by organic ions which make the interlayer spaces hydrophobic [9-10] and more sensitive to heavy metal ions. These organoclays and organo/LDHs have applications in a wide range of organic pollution control fields. To the best of our knowledge, nickel removal by LDHs has not yet been investigated. In this study, hydrotalcite (LDH) is synthesized in carbonate form by the co-precipitation method [11] and modified/LDH is obtained by intercalation of oxalate anions (C₂O₄²⁻) into the interlayer space of the hydrotalcite by direct anion exchange from the LDH precursor. The adsorption of nickel (II) by the obtained intercalated LDH material is then optimized.

2. Materials and method

2.1. Synthesis of the Mg/Al LDH

A co-precipitation and crystallization method [10], [12-13] was used to prepare the hydrotalcite in carbonate form (Mg₂AlCO₃-LDH). X-ray diffraction (XRD), FT-IR spectroscopy and thermogravimetric analysis were used to characterize the synthesized product.

2.2. Intercalation of C₂O₄²⁻ into the LDH

Iyi et al. (2011) [14] using aqueous HCl/NaCl solution succeeded in deintercalating CO₃²⁻ from CO₃-LDH and replacing it by Cl⁻ without any weight loss or morphological change under optimum conditions. The same method (anion exchange method) is used in this paper to intercalate oxalate anions into the interlayer of the synthesized precursor Mg₂AlCO₃-LDH, by using

$\text{Na}_2\text{C}_2\text{O}_4/\text{H}_2\text{C}_2\text{O}_4 \cdot 2\text{H}_2\text{O}$ solution. The modified Mg/Al LDH (henceforth designated as $\text{Mg}_2\text{AlC}_2\text{O}_4\text{-LDH}$) was then characterized by X-ray diffraction and FT-IR spectroscopy.

2.3. Characterization techniques

X-ray powder profiles were collected using a Bruker D5005 X-ray diffractometer equipped with sealed Cu- K_α radiation source ($\lambda_\alpha = 1.54184 \text{ \AA}$).

Thermogravimetric analyses (TGA) were carried out using a Perkin-Elmer thermogravimetric/differential thermal analyzer (TG/DTA). The measurements were recorded from 30 °C and 600 °C under nitrogen flow (100 mL.min⁻¹) with a heating rate of 10° C min⁻¹.

FT-IR spectra were obtained from pellets containing about 5% dried solid in KBr. The spectra were recorded between 4000 and 400 cm⁻¹ with a FT-IR Bruker.

2.4. Adsorption experiments

Aqueous solutions of nickel were prepared by dissolving nickel nitrate $\text{Ni}(\text{NO}_3)_2 \cdot 6\text{H}_2\text{O}$ in double distilled water. The pH of the solutions was adjusted using 0.01 M NaOH or 0.01 M HCl. All chemicals used were of analytical reagent grade. Nickel (II) analyses were done by a UV/Vis spectrophotometer (Jenway) at 395 nm.

Nickel adsorption was optimized by studying the influence of contact time, adsorbent dosage, pH of solution and initial concentration of nickel (II) ions. Kinetics and equilibrium models were also investigated. All the experiments were replicated thrice to assure the veracity of results.

The amount of Ni (II) absorbed per unit mass of adsorbent (Q_e) was calculated from equation 1:

$$Q_e = \frac{(C_0 - C_e)V}{m} \quad (1)$$

Where C_0 and C_e (mg/L) represent initial and equilibrium concentrations of metal ions in the aqueous phase respectively. V (L) is the volume of the solution and m (mg) is the mass of the adsorbent. The adsorption percentage (%R) of metal ions was calculated following equation 2:

$$(\%R) = \frac{(C_0 - C_e)100}{C_0} \quad (2)$$

To optimize the contact time, 5 mg of $\text{Mg}_2\text{AlC}_2\text{O}_4\text{-LDH}$ was stirred in 25 mL of a 2100 mg/L nickel solution at different time intervals (5-120 min).

To determine the influence of pH, experiments were performed at initial pH values ranging from 2 to 9. Initial concentration of 2100 mg/L nickel (II) and 5 mg of $\text{Mg}_2\text{AlC}_2\text{O}_4\text{-LDH}$ in 25 mL of solution were used for this purpose. The effect of initial metal ion concentrations was carried out by shaking (at the optimum contact time) 25 mL nickel (II) solutions of desired concentrations (800-2600 mg/L) with 5 mg of the adsorbent. All the samples were adjusted to the optimum pH prior to the addition of the adsorbent. The best amount of LDH was determined by treating different masses of the adsorbents ranging from 5 to 40 mg with 25 mL solution of the Ni (II) ions of initial concentration 2100 mg/L.

2.5. Kinetic modeling

Three kinetic models have been tested in the present study: pseudo-first order kinetic model, pseudo-second order kinetic model and Elovich model.

2.5.1. Pseudo-first order kinetic model

The pseudo first order equation was suggested by Lagergren (1898) [15] for the adsorption of solid-liquid systems. This model is based on the assumption that the adsorption rate is proportional to the number of available sites [16]

$$\frac{dQ_t}{dt} = K_1(Q_E - Q_t) \quad (3)$$

Where, Q_E and Q_t (mg/g) are the adsorption capacities at equilibrium and at time t respectively, K_1 (min⁻¹) being the rate constant of pseudo-first order adsorption. Equation 3 can also be written as follows after integration:

$$\ln(Q_E - Q_t) = \ln Q_E - K_1 t \quad (4)$$

2.5.2. Pseudo-second order model

This model is based on the assumption that adsorption rate is proportional to the square of the number of unoccupied sites [17]. The characteristic equation of this model is:

$$\frac{dQ_t}{dt} = K_2(Q_E - Q_t)^2 \quad (5)$$

Which is better written as:

$$\frac{t}{Q_t} = \frac{1}{K_2 Q_E^2} + \frac{t}{Q_E} \quad (6)$$

K_2 being the rate constant for the pseudo-second order adsorption (g/mg.min).

2.5.3. The Elovich kinetic model

This model is characterized by the following equation:

$$\frac{dQ_t}{dt} = \alpha \exp(\beta Q_t) \quad (7)$$

Where α (mg.g⁻¹.min⁻¹) and β (g.min⁻¹) are the initial adsorption rate and the desorption constant respectively. After integration, equation 7 becomes:

$$Q_t = \frac{1}{\beta} \ln(\alpha\beta) + \frac{1}{\beta} \ln t \quad (8)$$

2.6. Adsorption isotherms

The characteristic equation of Langmuir model is expressed as:

$$Q_E = Q_m \frac{K_L C_E}{1 + K_L C_E} \quad (9)$$

Where Q_E (mg/g) is the equilibrium metal ion concentration on the adsorbent, C_E (mg/L) the equilibrium metal ion concentration in the solution, Q_m (mg/g) the monolayer adsorption capacity of the adsorbent and K_L (L/mg) the Langmuir adsorption constant, related to the free energy of adsorption. This equation, reduced to its linear form, becomes:

$$\frac{C_E}{Q_E} = \frac{1}{Q_m K_L} + \frac{C_E}{Q_m} \quad (10)$$

The Freundlich model is applied in the case of non-ideal sorption on heterogeneous surfaces and multilayer sorption [18]. The equation is commonly given by:

$$\ln Q_E = \ln K_F + \frac{1}{n} \ln C_E \quad (11)$$

Where K_F is a constant related to the adsorption capacity and $\frac{1}{n}$ is an empirical parameter related to the adsorption intensity, which varies with the heterogeneity of the material.

3. Results and discussion

3.1. Characterization of materials

3.1.1. XRD analysis of pristine and modified LDH

The diffraction patterns of the pristine and modified LDH are shown in Fig 1. The diffractogram of the precursor material (Mg_2AlCO_3 -LDH) (Fig.1a) consisted of both sharp and symmetrical peaks and some high angle asymmetrical peaks; this provides evidence of well crystallized and ordered layered structure of Mg_2AlCO_3 -LDH. The typical pattern of hydrotalcite is present, that is a set of four reflection lines at $2\theta=10, 20.00, 38.56$ and 61.00° due to the reflections of the basal planes (003), (006), (015) and (110) respectively [19]. The Mg_2AlCO_3 -LDH spacing (that is, the thickness of a layer plus the interlayer space) is 8.77 \AA (Fig. 1a), value greater than that of a hydrotalcite of this type which is normally 7.65 \AA . This is reminiscent of a co-intercalation of larger anions in addition to carbonate ions, given their high concentration in the medium [20].

The XRD peaks of the modified material with oxalate ions are broad and generally less intense compared to the pristine LDH, suggesting a partial loss of crystallinity in the clay mineral due to the presence of the oxalate ions (Fig. 1b). It should be noticed that, the maximum peak due to the diffraction by basal plane (003) shifts towards lower diffraction angles; several harmonics are recorded and the d-spacing values increased; $9, 87 \text{ \AA}$ after the anionic exchange. The peak shift at $2\theta = 10$, indicates the CO_3^{2-} replacement by oxalate anions in the hydrotalcite interlayer [21]. From these results, it can be concluded that the oxalate anions have been intercalated into the gallery of LDH with large interlayer separation.

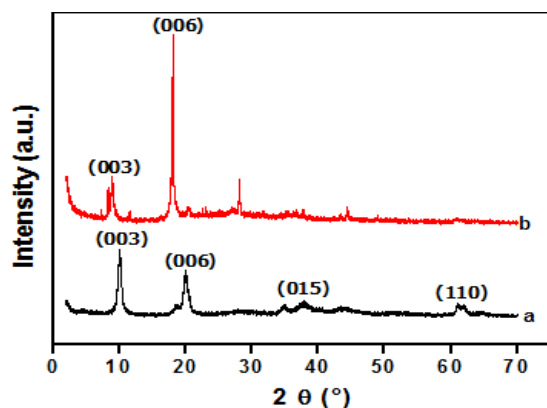


Fig. 1: (A) XRD Pattern of the Synthesized Mg_2AlCO_3 -LDH. (B) XRD Pattern of the Chemically Modified $Mg_2AlC_2O_4$ -LDH.

3.1.2. FT-IR analysis of the Mg_2AlCO_3 -LDH and $Mg_2AlC_2O_4$ -LDH materials

The FT-IR spectra of the LDH materials are shown in Fig. 2 and 3. All samples exhibited a very intense absorption band between 3200 and 3500 cm^{-1} due to the stretching mode of hydroxyl groups. This band is very broad, as it involves the vibration of the layer hydroxyl groups, as well as the stretching mode of interlayer water molecules. Hydrogen bonding between the water molecules and the interlayer anions also accounts for the broadening of this band. The bending mode of water gives rise to a rather weak band around 1625 - 1643 cm^{-1} [21-22]. In FT-IR spectra of the Mg_2AlCO_3 -LDH (Fig. 2), the IR absorptions due to the ν_3 and ν_4 stretching vibrations of interlayer CO_3^{2-} ions were recorded at

1340 - 1370 and 1000 - 1020 cm^{-1} . This is almost what is observed for every hydroxide irrespective of the nature of the octahedral sheets suggesting a rather symmetric environment for the interlayer anions [17], [18]. In the low frequency region, the adsorption peaks of the spectra corresponding to the lattice vibration modes are attributed to Mg-OH at 610 - 620 cm^{-1} , Al-OH at 540 - 780 cm^{-1} and O-Al-Mg-O at 440 - 550 cm^{-1} . The presence of oxalate anions in the LDH precursor was confirmed by the presence of three bands between 1550 and 1365 cm^{-1} (Fig. 3), which could be assigned to the stretching modes of the carboxylate group. Furthermore, the moderately intense bands in the 820 - 960 and 440 - 650 cm^{-1} range were typically attributed to the [O-C-O] stretching mode from the carboxylic acid (Coronado et al., 2010). In addition, the very strong absorption peak of the carbonate anions present in Fig. 2 disappeared or decreased after the ion-exchanged reaction (Fig. 3). This supports the idea that $C_2O_4^{2-}$ anions replaced the interlamellar CO_3^{2-} anions, as the X-ray analysis previously showed.

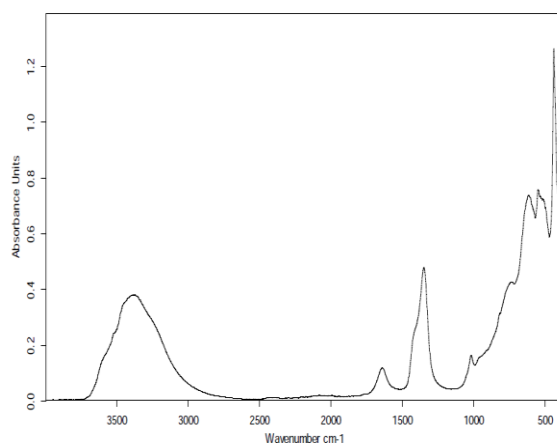


Fig. 2: FT-IR Spectrum of Mg_2AlCO_3 -LDH.

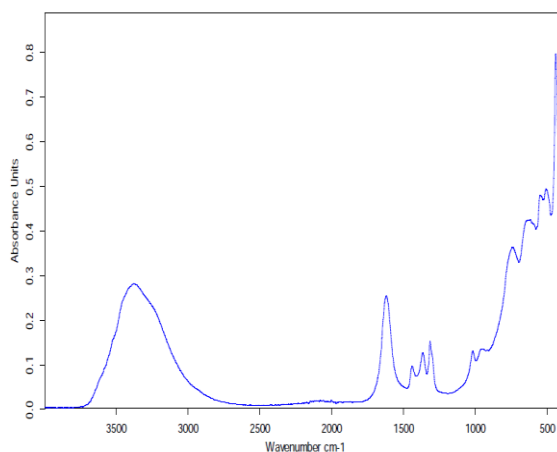


Fig. 3: FT-IR Spectrum of $Mg_2AlC_2O_4$.

3.1.3. Thermal analysis

Despite the diversity in composition, most LDHs exhibit similar thermal decomposition behavior. When heated, LDH releases interlayer water up to $250 \text{ }^\circ\text{C}$, followed by dehydroxylation of the hydroxide layers and decomposition of the interlayer anions at higher temperatures [22-23]. TGA, DTG and DTA curves of Mg_2AlCO_3 -LDH are given in Fig. 4. The DTA curves of pristine LDH show three major endothermic peaks in the intervals between (150 - $250 \text{ }^\circ\text{C}$), (250 - $450 \text{ }^\circ\text{C}$) and (450 - $650 \text{ }^\circ\text{C}$). Three major mass losses of Mg_2AlCO_3 -LDH with corresponding peaks around $122, 358,$ and $505 \text{ }^\circ\text{C}$ on the DTG diagram were observed in Figure 4c, which is consistent with the data reported in the literature [11]. The first step with a mass loss of $(12 \pm 1\%)$ at $122 \text{ }^\circ\text{C}$ is mainly ascribable to the removal of water, probably physisorbed on the external surface of the particles, as well as water molecules from

the interlayer space. The second and third steps, between 250 and 650 °C, are probably caused by both dehydroxylation of the hydroxide layers and expulsion of the intercalated carbonate anions. In some cases, the second peak splits into two peaks, the first of which corresponds to the loss of hydroxyl groups bound to Al, while the second of the split peaks represents the loss of hydroxyl groups bound to Mg together with decomposition of carbonate anions. No distinct mass loss can be observed on further calcinations above 650 °C, implying that the metal oxides of Mg_2AlCO_3-LDH can be produced above this temperature [10].

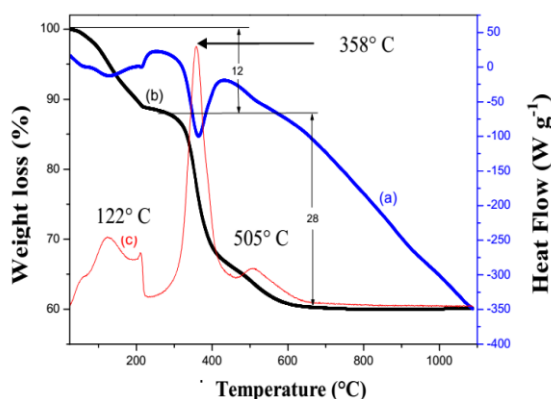


Fig. 4: (A) Differential Thermal Analysis (DTA) (Blue-Line), (B) Thermogravimetric Analysis (TGA) (Black Line) and (C) Derivative Weight (DTG) (Red-Line) Curves Performed under N_2 Atmosphere of Mg_2AlCO_3-LDH .

3.2. Adsorption properties of the pristine and modified LDHs

Fig.5 presents the adsorption capacity of the pristine and modified LDH obtained at pH 5 after addition of 5 mg of each synthesized material in 25 ml of 2100 mg/L nickel (II), and the mixture stirred for 15 min. Each adsorption capacity experiment was carried out in triplicate, and the average was considered.

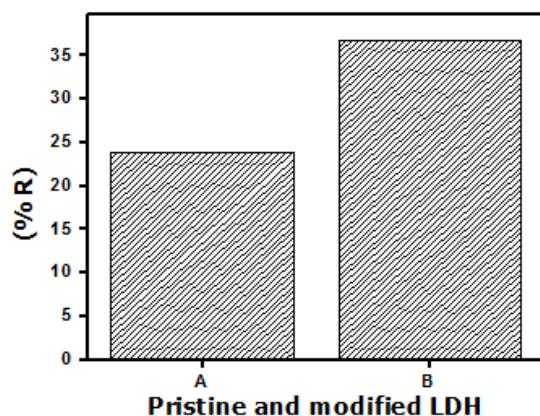


Fig. 5: Adsorption Capacity of Mg_2AlCO_3-LDH (A) and $Mg_2AlC_2O_4-LDH$ (B).

Under the same conditions, the adsorption capacity of $Mg_2AlC_2O_4-LDH$ (35%) is higher than that of the original LDH (23%). This is due to the expansion of the interlayer space of the former and the complexation of nickel ions by the oxalate ions [9], [14].

3.2.1. Effect of contact time

The adsorption of nickel (II) by $Mg_2AlC_2O_4-LDH$ (Fig. 6) occurs in two steps: a fast stage which takes 20 min with 28% yield and a slow step which takes 30 min with only 26% yield. Thus the equilibrium is reached after 50 min, contact time considered optimal for the subsequent experiments.

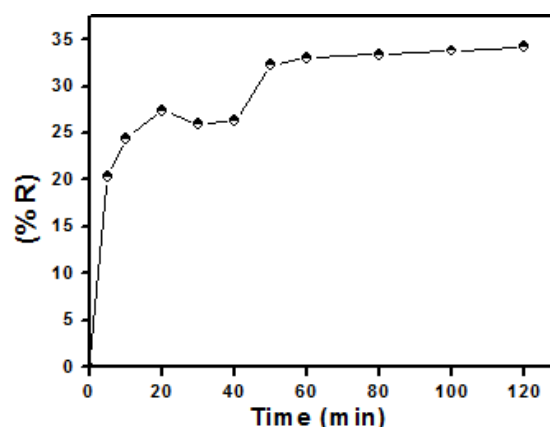


Fig. 6: Effect of Contact Time on Ni^{2+} Removal: 5.0 Mg $Mg_2AlC_2O_4-LDH$; 25 Ml of 2100 $Mg L^{-1} Ni^{2+}$; pH 5.0; Stirring Speed 150 Rpm, Ambient Temperature.

3.2.2. Effect of pH on Ni (II) adsorption

Fig. 7 shows the influence of pH on the adsorption of nickel ions. The low adsorption observed at pH 2 is due to the higher mobility of H^+ ions, promoting H^+ adsorption at the expense of nickel ions. The maximum adsorption observed in the pH range 4.5 - 6 might be due to partial hydrolysis of metal ions, resulting in the formation of $M(OH)^+$ ions which would be adsorbed to a greater extent on the surface of the adsorbents compared to M^{2+} ions. At higher pH values (above 6), precipitation is dominant or both ion exchange and aqueous metal hydroxide formation may become significant mechanisms in the metal removal process. Thus, all subsequent sorption experiments in this study were conducted at pH 6.0.

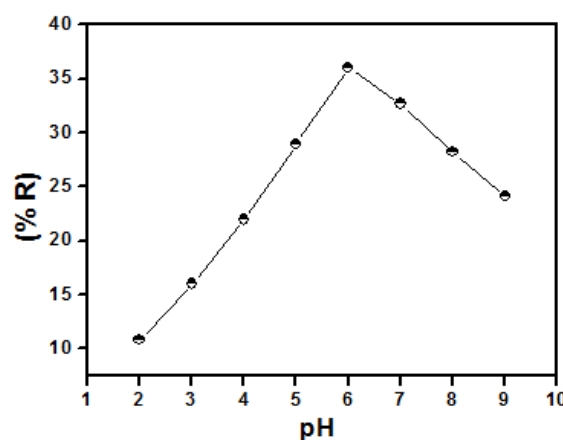


Fig. 7: Effect of pH on Ni^{2+} Removal: 5.0 Mg $Mg_2AlC_2O_4-LDH$; 25 Ml of 2100 $Mg L^{-1} Ni^{2+}$; Contact Time 50 Min; Stirring Speed 150 Rpm; Ambient Temperature.

3.2.3. Effect of adsorbent dosage

It appears on Fig. 8 that for an adsorbent mass between 5 and 35 mg, the adsorption percentage increases with increasing adsorbent dosage from 25 to 91%. Indeed, with an increase in the adsorbent dosage, more adsorbent surface is available for the adsorbate. On the other hand, the increase of adsorbent dose leads to the increase of oxalate ions amount and therefore, to an increased complexation of the adsorbate by the adsorbent, which ameliorates the percentage removal. However, the adsorption percentage becomes almost constant after addition of 20 mg of adsorbent. This result suggest that after a certain dose of adsorbent, the adsorption of metal ion reaches maximum and hence the amount of ions bound on the adsorbent site and the amount of free ions in the solution remain constant with further increase in the adsorbent dose [24].

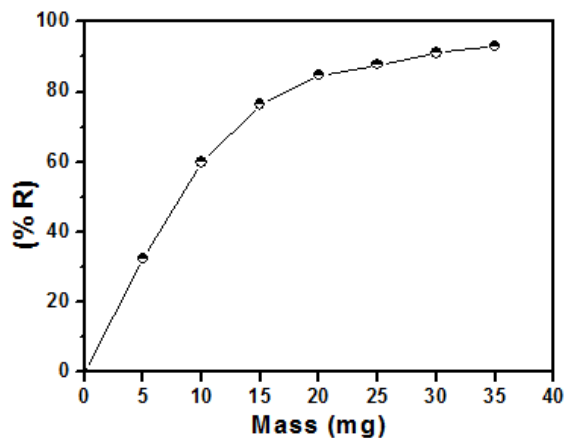


Fig. 8: Effect of Adsorbent Dosage ($\text{Mg}_2\text{AlC}_2\text{O}_4\text{-LDH}$) on Ni^{2+} Removal: 25 ml of 2100 mg L^{-1} Ni^{2+} ; pH = 6.0; Contact Time 50 Min; Stirring Speed 150 Rpm; Ambient Temperature.

3.2.4. Effect of initial metal ion concentration

Fig. 9 shows the effect of initial metal ion concentration on Ni^{2+} removal: the adsorption of Ni (II) decreases from 55% to 21% with increase in metal concentration from 800 to 3200 mg L^{-1} . So, at lower concentrations, the synthesized $\text{Mg}_2\text{AlC}_2\text{O}_4\text{-LDH}$ material is able to remove large amounts of Ni^{2+} from solution. At higher concentration, most of the Ni (II) are left unabsorbed due to the saturation of adsorption sites and the lack of sufficient surface area to accommodate much more metal available in solution.

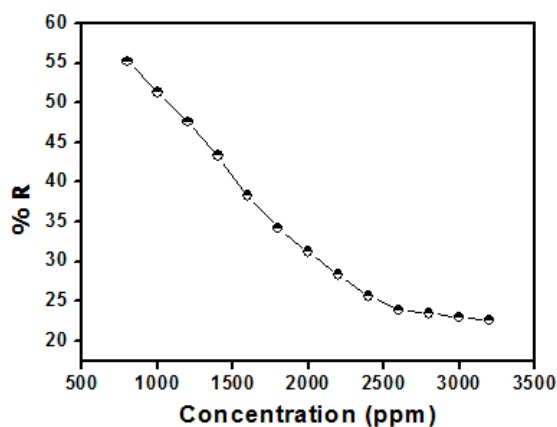


Fig. 9: Effect of Initial Metal Ion Concentration on Ni^{2+} Removal: 5 $\text{Mg Mg}_2\text{AlC}_2\text{O}_4\text{-LDH}$; pH = 6.0, Contact Time = 50 Min, Stirring Speed = 150 Rpm, Ambient Temperature.

3.3. Determination of adsorption isotherms

Adsorption isotherms of nickel (II) ions on the modified LDH are shown in Fig. 10. Linear plots of Langmuir and Freundlich isotherms are shown in Fig. 13 and 14. The values of Langmuir and Freundlich constants are reported in Table 1.

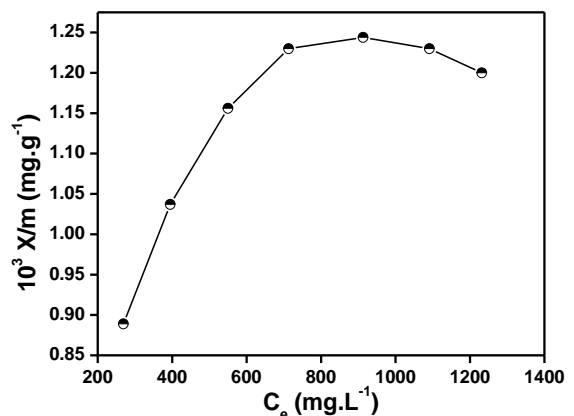


Fig. 10: Adsorption Isotherms of Ni^{2+} on 5 $\text{Mg Mg}_2\text{AlC}_2\text{O}_4\text{-LDH}$: pH 6.0, Contact Time 50 Min; Stirring Speed 150 Rpm, Ambient Temperature.

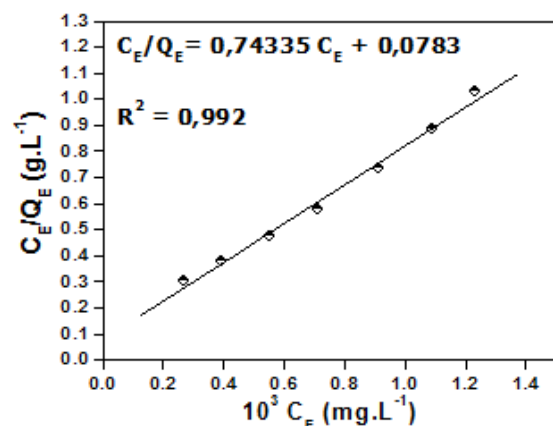


Fig. 11: Linear Plot of Langmuir Model: 5 $\text{Mg Mg}_2\text{AlC}_2\text{O}_4\text{-LDH}$: pH 6.0, Contact Time 50 Min; Stirring Speed 150 Rpm, Ambient Temperature.

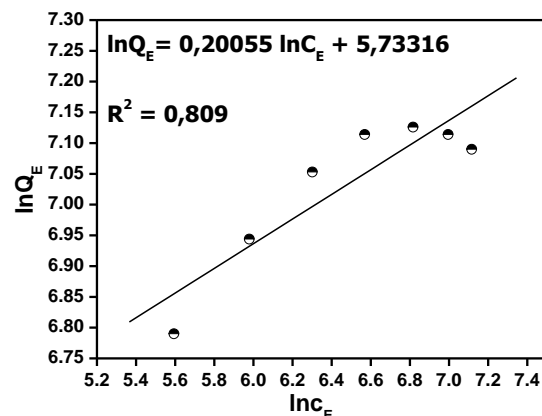


Fig. 12: Linear Plot of Freundlich Model: 5 $\text{Mg Mg}_2\text{AlC}_2\text{O}_4\text{-LDH}$: pH 6.0, Contact Time 50 Min, Stirring Speed 150 Rpm, Ambient Temperature.

Table 1: Isotherm Constants and Correlation Coefficients for Freundlich and Langmuir Models

Isotherm models	Freundlich			Langmuir		
	K_F	$1/n$	R^2	K_L (L/mg)	Q_m (mg/g)	R^2
$\text{Mg}_2\text{AlC}_2\text{O}_4\text{-LDH}$	308.940	0.20055	0.809	9.749	1310	0.992

The Langmuir model (Fig. 11) best describes the adsorption of nickel by $\text{Mg}_2\text{AlC}_2\text{O}_4\text{-LDH}$ ($R^2 = 0.992$). The maximum adsorption capacity Q_m is quite high (1310 mg/g , Table 1), proof that the modified LDH has a high capacity to adsorb nickel (II) ions. Also, the value of K_L which represents the energy of adsorption can also be considered as high, indicating that the adsorbent and the adsorbate form relatively stable attachments to each other [25]. As the Langmuir isotherm fits the experimental data very well, the

distribution of active sites on the adsorbent surface is homogeneous, reflecting the monolayer coverage of nickel (II) ions on its outer surface [26].

3.4. Kinetic modeling of Ni (II) adsorption

Adsorption kinetics of metal transport onto an adsorbent can be controlled by several independent processes. These are (i) bulk diffusion (ii) external mass transfer (film diffusion) (iii) chemical reaction (chemisorption) and (iv) inter-particle diffusion. These processes can act in series or parallel to account for the surface transport of a metal into an adsorbent [27]. The pseudo first-order and pseudo-second order kinetic models, and the Elovich model were enlisted to assess the nickel (II) adsorption mode (Figs. 13, 14, 15). Characteristic parameters of each kinetic model are given in Table 2.

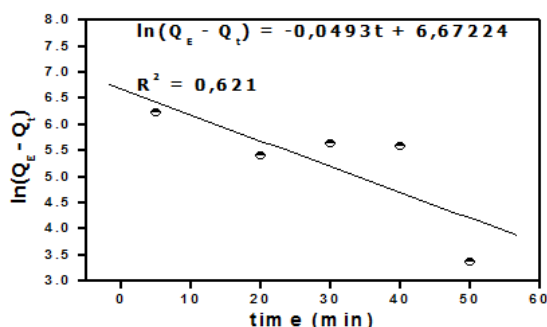


Fig. 13: Linear Pseudo-First Order Kinetic Model: 2100 Mg/L Ni²⁺, pH = 6.0, Stirring Speed 150 Rpm, Ambient Temperature.

Adsorbent	Mg ₂ AlC ₂ O ₄ -LDH	
C ₀ en mg.L ⁻¹	2100	
pseudo first-order	K ₁ .min ⁻¹	0.0493
	Q _e (mg.g ⁻¹)	790.16
	R ²	0.621
pseudo-second-order	10 ⁻³ K ₂ (g.min ⁻¹ mg ⁻¹)	0.08493
	10 ⁻² Q _e (mg.g ⁻¹)	14.37242
	R ²	0.992
	10 ³ h	0.17544
	α (mg.g ⁻¹ .min ⁻¹)	2.28206 x 10 ³
Elovich	β (g.mg ⁻¹)	0.00556
	R ²	0.860

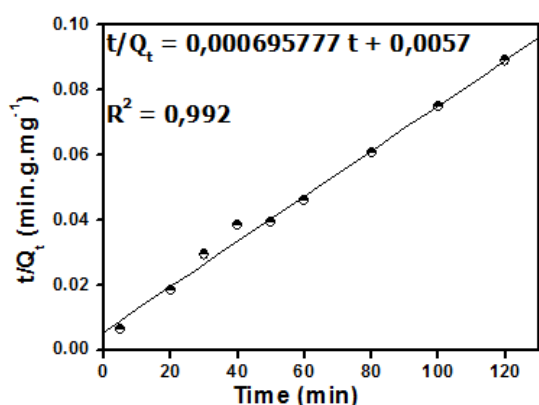


Fig. 14: Linear Pseudo-Second Order Kinetic Model: 2100 Mg/L Ni²⁺, pH = 6.0, Stirring Speed = 150 Rpm, Ambient Temperature.

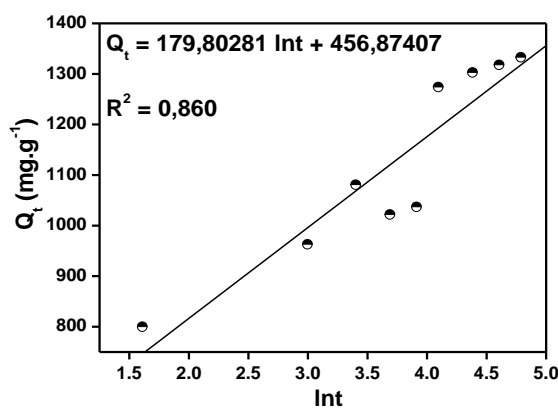


Fig. 15: Linear Elovich Kinetic Model: 2100 Mg/L Ni²⁺, pH = 6.0, Stirring Speed = 150 Rpm, Ambient Temperature.

The adsorption of Ni²⁺ ions by modified LDH follows the pseudo-second order kinetic model (R² = 0.992, Fig. 13). Consequently, chemisorption is the rate-limiting step.

4. Conclusion

In this study, two lamellar double hydroxides Mg₂AlCO₃-LDH and Mg₂AlC₂O₄-LDH were successfully synthesized through coprecipitation and anion exchange methods. These materials were characterized by X-ray diffraction, FT-IR spectroscopy and thermal analysis. LDH intercalated with oxalate ions was then applied to the adsorption of Ni (II). Optimization of adsorption parameters led to the following conclusions: the adsorption rate decreased with increase in initial metal ion concentration while it increased with increase in adsorbent dose; nickel removal is maximum (1310 mg/g) at pH 6.0 after 50 minutes of stirring at the rate of 150 rpm. Adsorption follows Langmuir model and pseudo-second order kinetic model. The interest of this study is that, the LDH intercalated by oxalate ions can be applied to the removal of many other heavy metals in solution.

Acknowledgement

We thank the Ministry of Higher Education of Cameroon for the special premium paid quarterly to Lecturers. The International Union of Crystallography (IUCr) and BRUKER AXS S.A.S France are thanked for the donation of diffractometer D5005 to the University of Dschang.

References

- [1] Das, K. K.; Das, S. N. & Dhundasi S. A. (2008). Nickel, its adverse health effects & oxidative stress. Indian Journal of Medicine Research, 128, 412-425.
- [2] ATSDR (Agency for Toxic Substances and Disease Registry), (1988). Toxicological profile for nickel, Atlanta, GA, USA: ATSDR/ U.S. Public Health Service, ATSDR/TP-88/19.
- [3] Coogan, T. P.; Latta, D. M.; Snow, E. T. & Costa, M. (1989). Toxicity and carcinogenicity of nickel compounds, in: McClellan RO, editor. Critical reviews in toxicology, Boca Raton, FL: CRC Press, 19, 341-384. <http://dx.doi.org/10.3109/10408448909029327>.
- [4] Xiang Z.; Jun M.; Xixin L.; Xiaoliu H.; Jing Z. (2015). High efficient removal of molybdenum from water by Fe₂(SO₄)₃: Effects of pH and affecting factors in the presence of co-existing background constituents. Journal of Hazardous Materials, 300, 823-829. <http://dx.doi.org/10.1016/j.jhazmat.2015.08.026>.
- [5] Lin, C.; Chengbin, L.; Guiyin, Z.; Rui, X.; Yanhong, T.; Zebing, Z. & Shenglian, L. (2015). A double network gel as low coast and easy recycle adsorbent: Highly efficient removal of Cd (II) and Pb (II) pollutants from wastewater. Journal of Hazardous Materials, 300, 153-160. <http://dx.doi.org/10.1016/j.jhazmat.2015.06.070>.
- [6] Bansal, M.; Singh, D.; Garg, V. K. & Rose, P. (2009). Use of Agricultural Waste for the Removal of nickel Ions from Aqueous Solu-

- tions: Equilibrium and Kinetics Studies. *International Journal of Civil and Environmental Engineering*, 2, 108-114.
- [7] Aisawa, S.; Shuji, S.; Satoshi, T.; Hidetoshi, H.; Hirokazu, N. & Eiichi, N. (2006). Intercalation of amino acids and oligopeptides into Zn-Al layered double hydroxide by coprecipitation reaction. *Journal of Physics and Chemistry of Solids*, 67, 920-925. <http://dx.doi.org/10.1016/j.jpics.2006.01.004>.
- [8] Chaara, D.; Bruna, F.; Ulibarri, M. A.; Draoui, K.; Barriga, C. & Pavlovic, I. (2011). Organo/layered double hydroxide nanohybrids used to remove nonionic pesticides. *Journal of Hazardous Materials*, 196, 350-359.
- [9] Ulibarri, M. A.; Pavlovic, I.; Barriga, C.; Hermosin M. C. & Cornejo, J. (2001). Adsorption of anionic species on hydrotalcite-like compounds: effect of interlayer anion and crystallinity. *Applied Clay Science*, 18, 17-27. [http://dx.doi.org/10.1016/S0169-1317\(00\)00026-0](http://dx.doi.org/10.1016/S0169-1317(00)00026-0).
- [10] Forano, C., Hibino, T., F. Leroux, F. & Gueho, T. C (2006). Layered double hydroxides. *Handbook of Clay Science*, 1, 1021-1095. [http://dx.doi.org/10.1016/S1572-4352\(05\)01039-1](http://dx.doi.org/10.1016/S1572-4352(05)01039-1).
- [11] Chiang, F. M. & Wu, M. T. (2011). Intercalation of γ -PGA in Mg/Al layered double hydroxides: An in situ WAXD and FTIR investigation. *Applied Clay Science*, 51, 330-334. <http://dx.doi.org/10.1016/j.clay.2010.12.021>.
- [12] Sommella, A.; Caporale, A.G.; Denecke, M.A; Mangold, S.; Pigna, M.; Santoro, A.; Violante, A. (2015). Nature and reactivity of layered double hydroxides formed by coprecipitating Mg, Al and As (V): Effect of arsenic concentration, pH, and aging. *Journal of Hazardous Materials*, 300, 504-512. <http://dx.doi.org/10.1016/j.jhazmat.2015.07.046>.
- [13] Klumpp, E.; Ortega, C. C.; Klahre, P.; Tino, F. J.; Yapar, S.; Portillo, C.; Stegen, S.; Queirolo, F. & Schwuger, M. J. (2004). Sorption of 2, 4-dichlorophenol on modified hydrotalcites. *Colloids and Surfaces A: Physicochem England Aspects*, 230, 111-116. <http://dx.doi.org/10.1016/j.colsurfa.2003.09.018>.
- [14] Iyi, N.; Yamada, H. & Sasaki, T. (2011). Deintercalation of carbonate ions from carbonate-type layered double hydroxides (LDHs) using acid alcohol mixed solutions. *Applied Clay Science*, 54, 132-137. <http://dx.doi.org/10.1016/j.clay.2011.07.017>.
- [15] Lagergren S. (1898). Zur theorie der sogenannten adsorption gelöster stoffe. *Kungliga Svenska Vetenskapens Handlingar*, Band 24, N^o4, 1-39.
- [16] Onundi, Y. B.; Mamun, A. A.; Khatib, A. M. F. & Ahmed, Y. M. (2010). Adsorption of copper, nickel and lead ions from synthetic semiconductor industrial wastewater by palm shell activated carbon. *International Journal of Environmental Science and Technology*, 4, 751-758. <http://dx.doi.org/10.1007/BF03326184>.
- [17] Ho, Y. S. (2006). Review of second-order models for adsorption systems. *Journal of Hazardous Materials*, 136, 681-689. <http://dx.doi.org/10.1016/j.jhazmat.2005.12.043>.
- [18] Tancredi, N.; Medero, N.; Möller, F.; Pfriz, J.; Plada, C. & Cordero, T. (2004). Phenol adsorption on to powdered and granular activated carbon prepared from Eucalyptus wood. *Journal of Colloid and Interface Science*, 279, 357-363. <http://dx.doi.org/10.1016/j.jcis.2004.06.067>.
- [19] Yin, H.; Cui, L.; Ai, S.; Fan, H. & Zhu, L. (2010). Electrochemical determination of bisphenol A at Mg-AlCO₃ layered double hydroxide modified glassy carbon electrode. *Electrochimica Acta*, 55, 603-610. <http://dx.doi.org/10.1016/j.electacta.2009.09.020>.
- [20] Assaker, B. I. (2009). Synthèse électrochimique de films d'hydroxydes doubles lamellaires - application aux biocapteurs. Thèse de Doctorat, Université d'Evry Val d'Essonne, Essonne, France.
- [21] Fernández, L.; Borrás, C. & Carrero H. (2006). Electrochemical behavior of phenol in alkaline media at hydrotalcite-like clay/anionic surfactants/glassy carbon modified electrode. *Electrochimica Acta*, 52, 872-884. <http://dx.doi.org/10.1016/j.electacta.2006.06.021>.
- [22] Pérez, M. R.; Barriga, C.; Fernández, J. M.; Rives, V. & Ulibarri, M. A. (2007). Synthesis of Cd/ (Al+Fe) layered double hydroxides and characterization of the calcination products. *Journal of Solid State Chemistry*, 180, 3434-3442. <http://dx.doi.org/10.1016/j.jssc.2007.09.035>.
- [23] Coronado, E.; Gastaldo, M. C.; Moratalla, E. N. & Ribera, A. (2010). Intercalation of [M (ox)₃]³⁻ (M = Cr, Rh) complexes into Ni^{II}Fe^{III}-LDH. *Applied Clay Science*, 48, 228-234. <http://dx.doi.org/10.1016/j.clay.2009.11.054>.
- [24] Demirbaş, O.; Alkan, M.; Doğan, M.; Turhan, Y.; Namli, H. & Turan, P. (2007). Electrokinetic and adsorption properties of sepiolite modified by 3-aminopropyltriethoxysilane. *Journal of Hazardous Materials*, 149, 650-656. <http://dx.doi.org/10.1016/j.jhazmat.2007.04.036>.
- [25] Hasar, H. (2003). Adsorption of nickel (II) from aqueous solution onto activated carbon prepared from almond husk. *Journal of Hazardous Materials*, 97, 49-57. [http://dx.doi.org/10.1016/S0304-3894\(02\)00237-6](http://dx.doi.org/10.1016/S0304-3894(02)00237-6).
- [26] Pavan, A. F.; Lima, S.; Lima, E.C.; Airoldi, C.; Gushikem, Y. (2006). Use of Ponkan mandarin peels as biosorbent for toxic metals uptake from aqueous solutions. *Journal of Hazardous Materials*, 137(1), 527-533. <http://dx.doi.org/10.1016/j.jhazmat.2006.02.025>.
- [27] Idris, S.; Iyaka, Y. A.; Dauda, B. E. N.; Ndamitso, M. M. & Umar, M. T. (2012). Kinetic study of utilizing groundnut shell as an adsorbent in removing chromium and nickel from dye effluent. *American Chemical Science Journal*, 1, 12-24. <http://dx.doi.org/10.9734/ACSJ/2012/908>.